Model-informed design of antibiotic therapy against antimicrobial resistance

Tandar, S.T.

Chapter 6

Physiologically-based modelling framework for prediction of pulmonary pharmacokinetics of antimicrobial target site concentrations

Linda B. S. Aulin
Sebastian T. Tandar
Torben van Zijp
Etienne van Ballegooie
Piet H. van der Graaf
Mohammed A. A. Saleh
Pyry Välitalo
J. G. Coen van Hasselt

Clinical pharmacokinetics (2022). 61(12), 1735–1748.

Abstract

Prediction of antimicrobial target site pharmacokinetics is of relevance to optimize treatment with antimicrobial agents. A physiologically based pharmacokinetic (PBPK) model framework was developed for prediction of pulmonary pharmacokinetics, including key pulmonary infection sites, *i.e.* the alveolar macrophages and the epithelial lining fluid. The modelling framework incorporated three lung PBPK models: a general passive permeability-limited model, a drug-specific permeability-limited model, and a quantitative structure-property relationship (QSPR)-informed perfusion-limited model. We applied the modelling framework to three fluoroquinolone antibiotics. Incorporation of experimental drug-specific permeability data was found essential for accurate prediction. In the absence of drug-specific transport data, our QSPR-based model has generic applicability. We furthermore evaluated the impact of drug properties and pathophysiological related changes on pulmonary pharmacokinetics. Pulmonary pharmacokinetics was highly affected by physiological changes that cause a shift in the main route of paracellular or transcellular diffusion. Finally, we show that lysosomal trapping can cause an overestimation of cytosolic concentrations for basic compounds when measuring drug concentrations in cell homogenate. In conclusion, the developed lung PBPK model framework constitutes a promising tool for characterization of pulmonary exposure of systemically administrated antimicrobials.

Introduction

Consideration of antimicrobial target site concentration at the site of infection is crucial to derive treatment strategies with optimal efficacy and minimize the risk for antimicrobial resistance (AMR)[1]. For respiratory tract infections (RTIs), key target site include the epithelial lining fluid (ELF) and the alveolar macrophage (AM)[2]. Drug concentrations in ELF and AM may be significantly different compared to the plasma[3].

Systematically administered drugs pass through the pulmonary capillary wall, into the interstitial space, and cross the alveolar epithelium (**Fig. 1**). The alveolar epithelium acts as a semi-permeable barrier with tight junctions restricting paracellular diffusion[4] and active drug transporters[5]. For intracellular uptake of antibiotics in AMs, passage through the cell membrane by means of passive diffusion or active transport is needed. Intercellular pathogens in AMs localize in the cytosol, *i.e.* outside of the lysosomes. The low pH of lysosomes compared to the cytosol can alter the charge of molecules entering this compartment, causing lysosomal trapping[6], thereby decreasing the target site concentrations in AM cytosol. Together, these processes lead to target site concentrations in the ELF and AM that may de*via*te from plasma.

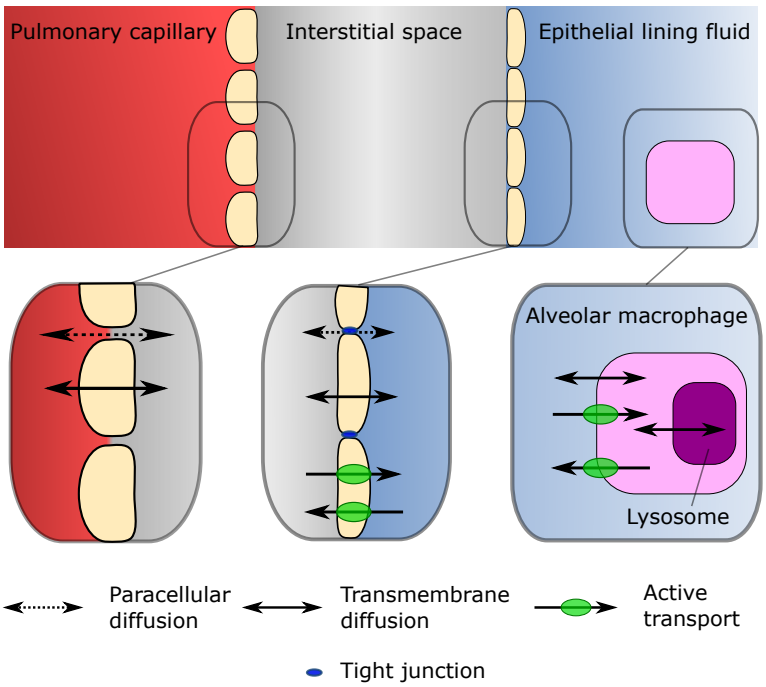

Fig. 1 | Overview of physiological lung compartments. Physiological compartments in the lung, their associated barriers, and the different modes of transport across specific barriers are shown.

Pathophysiological changes during infection, or due comorbidities, may lead to increased permeability over the alveolar epithelium[7], increased ELF volume[8], AM recruitment[9], and acidification of the ELF[10] and/or the interstitial fluid. Consequently, these pathophysiological changes may further alter the (expected) target site concentrations of antibiotics. However, pulmonary pharmacokinetics (PK) is currently under-studied in patients[2], typically relying on clinical studies in healthy volunteers[2].

The quantification of ELF and AM drug concentrations is typically achieved by bronchoalveolar lavage (BAL) sampling[2]. Commonly, only a single BAL is performed per subject and the method is associated with high measurement variability[11]. *In silico* modelling approaches predicting pulmonary drug exposure can thus provide valuable complementary insights. Here, quantitative structure-property relationship (QSPR)-based approaches are of interest to predict ELF-to-plasma ratio (EPR), based on chemical structural features alone[12,13]. However, QSPR models lack the ability to explore the full ELF PK and do not allow the evaluation of pathophysiological effects on PK. In this context, physiologically-based pharmacokinetics (PBPK) models can be of values as they allow for the prediction of drug concentration in physiological compartments based on physiological and drug-specific parameters.

Several lung PBPK models have been previously developed[14–16]. These models constitute important tools to predict drug PK in the ELF. However, they lack the representation of one of the key microbial infection sites, the AMs. In addition, the aforementioned PBPK models rely on *in vitro* or *in vivo* data of apparent permeability to describe drug transport over the alveolar epithelium. This limits previous models' applicability in cases where permeability data are lacking, which is often the case with novel compounds.

Here, we aimed to address these limitations by developing a novel lung PBPK model framework to predict PK of small molecule drugs at key target sites for RTIs, *i.e.*, ELF and AMs, accounting for spatial heterogeneity in lung physiology. Specifically, we developed and evaluated three complementary lung PBPK models for systemic antimicrobials, i) a general passive permeability-limited model, ii) a drug-specific permeability-limited model, iii) a QSPR-informed perfusion-limited model. We applied the different models to a fluoroquinolone data set. We then used the passive transport model to identify the main drug properties affecting pulmonary PK and evaluate the effect of pathophysiological changes.

Methods

The PBPK modelling and simulation framework relied on the integration of modular components that include the PBPK base model, and three alternative model implementations of the lung. The different lung PBPK models included different approaches of describing pulmonary drug transport: i) a general passive permeability-limited model, ii) a drug-specific permeability-limited model, iii) a QSPR-informed perfusion-limited model.

PBPK model structure

A minimal-PBPK model was developed which includes a physiological blood reservoir compartment, a physiological peripheral compartment, and a detailed physiological lung section. The base structure of the developed model is shown in **Fig. 2B**. The lung section represents the lower respiratory tract and was divided into six different zones to account for the spatial differences of the volume, surface area, and blood flow within and between the lungs. Each of the different lung zones were further divided into serially linked physiological compartments (**Fig. 2B**) and were aimed to describe ELF and AM concentrations. Blood-lung drug transport was implemented using three alternative models: i) a general passive permeability-limited model, ii) a drug-specific permeability-limited model, iii) a QSPR-informed perfusion-limited model.

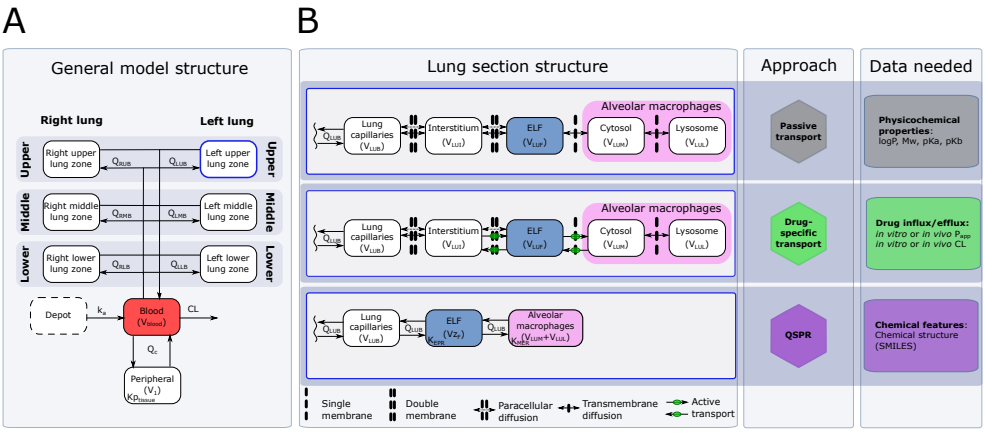

Fig. 2 | PBPK model structure and associated approaches and data requirements. **A.** General model structure of the minimal PBPK model including the lung section with the six different lung zones. The full cardiac output (Q_c) is heterogeneously divided over the different lung zones (z) to account for spatial difference in pulmonary blood flow (Q_{ZB}). The blood clearance (CL), blood-to-tissue partitioning for the peripheral compartment (Kp_{tissue}), and apparent absorption rate (k_a) are implemented as empirical parameters while the other included parameters are physiologically derived. **B.** Overview of three variations of the lung sub-model using different approaches to describe lung drug disposition and what data each approach required.

The permeability-limited models included five compartments for every lung zone, representing the lung capillaries, the interstitial space, the ELF, the AM cytosol, and the AM lysosomes. The perfusion-limited model included three compartments, representing the lung capillaries, the ELF, and the AMs, respectively. For all three models, only the free unbound drug was assumed to distribute from the pulmonary capillaries into the subsequent compartment. Protein binding was assumed negligible for all pulmonary non-blood compartments.

Blood drug disposition model. The drug disposition in the blood reservoir and peripheral compartment after intravenous administration was described by the following ordinary differential equations (**Eq. 1** and **Eq. 2**).

$$\frac{dA_{\text{blood}}}{dt} = Q_c \left(\frac{A_{\text{peripheral}}}{V_{\text{peripheral}} \times K_{p,\text{tissue}}} - \frac{A_{\text{blood}}}{V_{\text{blood}}} \right) + \sum \left(Q_{\text{ZB}} \times \frac{A_{\text{ZB}}}{V_{\text{ZB}}} \right) - \sum \left(Q_{\text{ZB}} \times \frac{A_{\text{blood}}}{V_{\text{blood}}} \right) - CL \times \frac{A_{\text{blood}}}{V_{\text{blood}}} \quad \textbf{Eq. 1}$$

$$\frac{dA_{\text{peripheral}}}{dt} = Q_c \left(\frac{A_{\text{blood}}}{V_{\text{blood}}} - \frac{A_{\text{peripheral}}}{V_{\text{peripheral}} \times K_{p,\text{tissue}}} \right) \quad \textbf{Eq. 2}$$

where A_{blood}, $A_{peripheral}$, and A_{ZB} and V_{blood}, $V_{peripheral}$, and V_{ZB} represents the amount of drug in the different compartments and their related volumes, respectively.

Additionally, CL represents the blood clearance, Kp_{tissue} the blood-to-tissue partitioning for the peripheral compartment, Q_c the cardiac output, and Q_{ZB} the zone-specific blood flow. Here, ZB is the pulmonary capillary compartment (B) of lung zone Z, which includes right upper, middle, and lower zone (R_{UB}, R_{MB}, and R_{LB}, respectively), and their left side counterparts (L_{UB}, L_{MB}, and L_{LB}). Oral drug administration was implemented using a depot compartment with a first-order apparent absorption rate (k_a).

Physiological parameters. The model framework was developed using a combination of empirically estimated plasma PK parameters including CL, Kp_{tissue}, and k_a, and physiological system-specific parameters derived from literature (**Table 1**). Briefly, the total body volume was derived from the bodyweight, assuming a density of 1 L/kg. The total volume was made up of the volume of the blood reservoir (7.71%[17]), the volume of the lower respiratory tract (0.63%[14,17]), and the residual volume associated with the peripheral compartment (91.7%). The volume related to the AMs (approximately 2 mL) was derived from the concentration of AMs in the ELF[11], the ELF volume[14], and the volume per-AM[18]. The total AM volume was divided over the cytosol and the lysosomes, which accounts for 92.2% and 7.8% of the total AM volume, respectively[6]. The AMs and lysosomes were assumed spherical and each AM contained one lysosome. The spatial difference in volumes, surface areas, and perfusion within the lower respiratory tract were implemented by relating factions of these to the left and right side[19], and further splitting those into upper, middle and lower lung zones[20].

The general passive permeability-limited model. Passive transport in the lung includes paracellular and transmembrane diffusion (**Fig. 1**). Transmembrane diffusion refers to the passive diffusion occurring through the phospholipid bilayers in the membrane of pulmonary capillary endothelial cells, the alveolar epithelium, and the AMs and their lysosomes. The transmembrane transport was implemented according to **Eq. 3**[21,22], where only the neutral fraction (NF) was assumed to be available for transmembrane transport.

$$\log P_{\mathrm{TM}} = 0.939 \times \log P - 6.210 \qquad \textbf{Eq. 3}$$

In **Eq. 3**, P_{TM} represents the transmembrane permeability (cm/s) over a single membrane and the n-octanol-water lipophilicity index (logP) the n-octanol lipophilicity index. For cell barriers, the transcellular permeability was obtained by dividing P_{TM} by two, thus accounting for the double membrane passage needed to pass through the cell.

The compartment specific NF of the drug was calculated using an adapted Henderson-Hasselbach equation (**Eq. 4**)[23], relating the neutral fraction of the strongest acidic group (NF_{acidic}) and the strongest basic group (NF_{basic}) of the drug according to **Eq. 5** and **Eq. 6**, respectively.

$$NF = NF_{\mathrm{acidic}} \times NF_{\mathrm{basic}} \qquad \textbf{Eq. 4}$$

$$NF_{\mathrm{acidic}} = \frac{1}{1 + 10^{\left(\mathrm{pH_{comp}} - \mathrm{p}K_a\right)}} \qquad \textbf{Eq. 5}$$

$$NF_{\mathrm{basic}} = \frac{1}{1 + 10^{\left(\mathrm{p}K_b - \mathrm{pH_{comp}}\right)}} \qquad \textbf{Eq. 6}$$

Table 1. System-specific parameters used in the PBPK model.

Parameter	Description	Value	Unit	Ref.
Q_c	Cardiac output	390	L/h	[17]
$F_{Q,\mathrm{Upper}}$	Fraction perfusing the upper lung	0.116		[20]
$F_{Q,\mathrm{Middle}}$	Fraction perfusing the middle lung	0.297		[20]
$F_{Q,\mathrm{Lower}}$	Fraction perfusing the lower lung	0.587		[20]
$F_{Q,\mathrm{Left}}$	Fraction perfusing the left lung	0.46		[19]
$F_{Q,\mathrm{Right}}$	Fraction perfusing the right lung	0.54		[19]
D_{Blood}	Volume blood per kg bodyweight	0.0771	L/kg	[17]
D_{Lung}	Volume lung per kg bodyweight	0.0076	L/kg	[17]
V_{PBR}	Total volume of blood in lung	89×10^{-3}	L	[14]
$F_{\mathrm{interstitium}}$	Fraction of lung volume equal to the interstitium volume	0.2		[23]
V_{ELF}	Total ELF volume	25	mL	[14]
$N_{\mathrm{AM,F}}$	Number of macrophages	1.99×10^{13}	cells/L	[11]
V_{AM}	Volume per macrophage	4989.9×10^{-15}	L	[18]
V_{Lys}	Volume per alveolar lysosome	0.0166×10^{-15}	L	[24]
F_{LRT}	Fraction of lung representing the lower respiratory tract	0.8333		[14]
$F_{V,\mathrm{Upper}}$	Split volume fraction	0.25		[25]
$F_{V,\mathrm{Middle}}$	Split volume fraction	0.36		[25]
$F_{V,\mathrm{Lower}}$	Split volume fraction	0.39		[25]
$F_{V,\mathrm{Right}}$	Split volume based on the lung side	0.5341		[25]
$F_{V,\mathrm{Left}}$	Split volume based on the lung side	0.4659		[25]
$F_{V,L}$	Lysosome fraction of total AM volume	0.078		[6]
A_{SA}	Alveolar epithelial surface area	130×10^2	dm^2	[26]
B_{SA}	Luminal capillary surface area	117×10^2	dm^2	[26]
$\mathrm{AM}_{\mathrm{SA}}$	Surface area per macrophage	1.39867×10^{-7}	dm^2	[18]
L_{SA}	Surface area per lysosome	14.6×10^{-11}	dm^2	[24]
Th_{B}	Thickness blood endothelial	0.46×10^{-5}	dm	[26]
Th_{A}	Thickness pneumocytes	0.3×10^{-5}	dm	[26]
$\mathrm{Pro}_{\mathrm{AM}}$	Protein per macrophage	107×10^{-9}	mg/cell	[27]
$\mathrm{pH}_{\mathrm{ELF}}$	pH in ELF	6.6		[10]
$\mathrm{pH}_{\mathrm{interstitium}}$	pH in interstitial fluid	7.4		[10]
$\mathrm{pH}_{\mathrm{cytosol}}$	pH in AM cytosol	7.2		[6]
$\mathrm{pH}_{\mathrm{lysosome}}$	pH in AM lysosomes	4.75		[6]
Pr_s	Pore size of small pores in epithelial tight junctions	0.32×10^{-8}	dm	[28]
Pr_l	Pore size of large pores in epithelial tight junctions	11.56×10^{-8}	dm	[28]
PA_s	Fraction of total alveolar area of small pores	3.03×10^{-3}		[28]
PA_l	Fraction of total alveolar area of large pores	7.90×10^{-7}		[28]

The surface area available for transmembrane transport over the luminal side of the capillaries was assumed to be 99.8% of the total surface area[22], while the remaining area was assumed to be paracellular space. The surface area of the alveolar epithelium available for transmembrane transport was assumed equal to the full alveolar surface area minus the total area of the aqueous pores in the tight junctions. The full surface area of the AMs and the lysosome were available for transmembrane transport.

The alveolar capillary wall is a highly permeable structure[24], and therefore the full paracellular space was assumed to be available for transport. Paracellular transport over the alveolar epithelium is restricted by tight junctions[24,25], and was assumed to only take place through aqueous pores present in tight junctions. Here, we assumed the presence of small pores with a radius of 0.32 nm (r_S) and large pores with a radius of 11.52 nm (r_L). These accounted for 0.303% and 0.00079% of the total alveolar surface area, respectively[25]. Passage was assumed to occur only for molecules with radius r smaller than the corresponding pore radius (r_S or r_L). Molecules that met the size criteria diffused according to **Eq. 7**[22,29] without any charge restriction.

$$\log D_{\text{aq}} = -4.11 - 0.4609 \times \log M_w \qquad \textbf{Eq. 7}$$

where D_{aq} is the aqueous diffusivity coefficient (cm^2/s), and MW is the molecular weight (g/mol). The molecular radius r was assumed to be constant and calculated according to the Stoke-Einstein equation (**Eq. 8**)[25,27].

$$r = \frac{k \times T}{6 \times \pi \times \eta \times D_{\text{aq}}} \qquad \textbf{Eq. 8}$$

where k is the Boltzmann constant (1.38×10^{-23} J/K), T is the absolute temperature (300 K), and η is the viscosity of water at 300 K ($0.69\ mPa \times s$).

The drug-specific permeability-limited model. We included the option to incorporate drug-specific influx and efflux over the alveolar epithelium and the macrophage membrane. The drug-specific transport was informed by literature data from *in vitro* permeability assays using human cultivated alveolar epithelial cells (Calu-3 cells) or rat AMs. The *in vitro* derived permeability was assumed to represent both active and passive transport processes.

The perfusion-limited QSPR-informed model. To allow for the structure based predictions of drug penetration into the ELF and the AM, we first fitted two QSPR-based elastic net regression models predicting the log steady-state concentration ratio for EPR and AM-ELF ratio (AM-ELF ratio (MER)) according to our previously described method[12]. Briefly, clinical data for 40 anti-infective agents on systemic and pulmonary exposure (ELF and AMs)[12] were extracted from literature and pre-processed as previously described[12]. The dataset was divided into a training (n = 32) and a test (n = 8) dataset for the development and validation of the QSPR models, respectively. The test dataset included the three fluoroquinolones used in our model application examples. Elastic net tuning was optimized by minimizing the root mean square error (RMSE) and leave-one-out cross-validation.

The QSPR-derived ratios were incorporated into the perfusion-limited model. The ratios were included as partitioning coefficients where the EPR and MER represented the partitioning of free drug between the plasma and ELF and the ELF and AMs, respectively.

Modelling framework applications

Application to fluoroquinolone antibiotics. We applied the framework to three fluoroquinolone antibiotics. We first digitized data from previous studies that repoted the steady-state lung concentrations of ciprofloxacin[28], grepafloxacin[30], and levofloxacin[31] (Table S1). The study-specific mean body weight was used to calculate physiological. We empirically derived the tissue-partitioning coefficient (Kp_{tissue}), the (apparent) plasma CL, and apparent absorption constant (k_a), when applicable, from the naïvely pooled observed plasma concentration data using nonlinear regression. We applied and compared the three different lung models, using the mean concentrations the different lung zones. Prediction performance was evaluated by calculating RMSE.

Exploring the effect of drug properties on pulmonary drug exposure. Using the passive model, we simulated treatments of different hypothetical antimicrobials to better understand how biological and drug specific properties (MW, logP, pk_a, pk_b) affect pulmonary PK. Specifically, we defined a comparator drug for each molecule, which had a CL of 10 L/h, Kp_{tissue} of 1, logP of zero, and MW of 500 g/mol. To allow for the evaluation of the impact of certain drug-specific parameters on pulmonary PK, we varied Kp_{tissue}, logP, and MW for three different drug molecules: one acid (pk_a = 4, pk_b = -3), one base (pk_a = 14, pk_b = 9), and one neutral (pk_a = 9, pk_b = -4).

For each tested drug, the steady-state maximum drug concentration (C_{max}) and 24-hour area under the concentration-time curve (AUC) were calculated. These exposure metrics were used to calculate the log2 ratio (L2R) of the metric of the specific drug x and its comparator according to **Eq. 9**, where metric is either steady-state AUC or C_{max}.

$$L2R_{metric,x} = \log_2\left(\frac{metric_x}{metric_{comparator}}\right) \qquad \textbf{Eq. 9}$$

Quantifying the effect of pathophysiology on pulmonary drug exposure

Pathophysiological changes can alter antimicrobial PK. To understand how such changes can influence pulmonary PK, we varied selected parameters known to be affected by infections. Using the passive model, we simulated treatments with a set of different hypothetical antimicrobials while increasing the ELF volume, the number of AMs, or the size of the small pores in the alveolar epithelium or decreasing the pH in the ELF or the interstitial fluid. To evaluate the effect of pathophysiology, we defined a base scenario for each different molecules, where the physiological parameters represent that of a healthy individual. The impact of pathophysiological changes was assessed for each drug by calculating the L2R of the metric (AUC or C_{max}) of the disease scenario and the base scenario (analogous to **Eq. 9**).

Software and model code

All PK analyses were performed in R (v. 4.0.5), using the packages 'nlmixr' (version 2.0.4) and 'RxODE' (version 1.0.8). All code related to the PBPK framework is available as supplementary information. The elastic net QSPR-models were developed using the R packages 'caret' (version 6.0-88), 'elasticnet' (version 1.3), and 'rcdk' (version 3.5.0).

Results

The developed QSPR-based models predict pulmonary drug penetration

Both of the fitted QSPR-based models performed adequately (**Fig. 3**). The EPR-model predicted the log steady-state ELF-to-Plasma ratio (log-EPR) well for the training (RMSE = 1.17, R^2 = 0.65) and acceptably for the test set (RMSE = 1.14, R^2 = 0.24). The log-EPR was 1.69, 1.53, and 1.47, for grepafloxacin, ciprofloxacin, and levofloxacin, respectively. Similarly, the MER-model could predict the log-AM-to-ELF ratio (log-MER) well for both the training (RMSE = 1.57, R^2 = 0.65) and the test set (RMSE = 2.03, R^2 = 0.49). The predicted log-MER for grepafloxacin, ciprofloxacin, and levofloxacin were 1.09, 0.84, and 1.21, respectively. The result from the optimization of tuning parameters can be seen in Fig. S1.

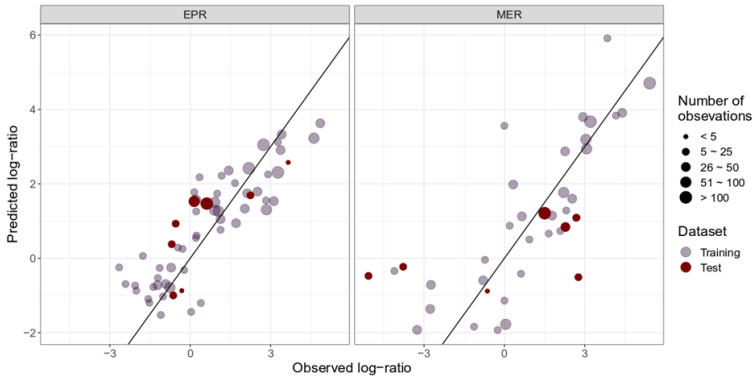

Fig. 3 | Performance of the developed QSPR models. Predicted versus observed log EPR and MER (130 structural features each). The hyperparameters s and λ were set to 0.20 and 0.10 for the EPR-model and 0.25 and 0.25 for the MER-model, respectively.

Prediction of fluoroquinolone lung PK

Plasma concentration data could be described well for all tested fluoroquinolone antibiotics (**Fig. 4**). Out of the three different lung models, the passive model performed the worst for all three antibiotics (**Fig. 4** and Fig. S2), with RMSE ranging between 0.98 to 2.39 and 1.86 to 4.73 for the ELF and AMs, respectively. The passive model predicted a very slow equilibration between the ELF and AMs, leading to a systematic under prediction of the AM concentrations. Overall, the approach using *in vitro* informed active transport outperformed the QSPR approach, except for the ELF prediction of grepafloxacin (RMSE 1.18 and 0.92 for active and QSPR approach, respectively) and AM prediction of levofloxacin (RMSE 0.59 and 0.58 for active and QSPR approach, respectively). Regardless of which approach used, there was no heterogeneity in the drug distribution into the different lung zones (data not shown).

Drug-specific effects

The investigation of how different drug-specific and empirical PK parameters influence the pulmonary PK revealed how molecules with different charges (*i.e.*, acid, base, or neutral) were affected differently (**Fig. 5**). Exposure at the AM compartment was more affected by logP when the drug was an acid or a base, as compared to a neutral compound. The Kp_{tissue} parameter affects drug distribution, and as such it had no effect

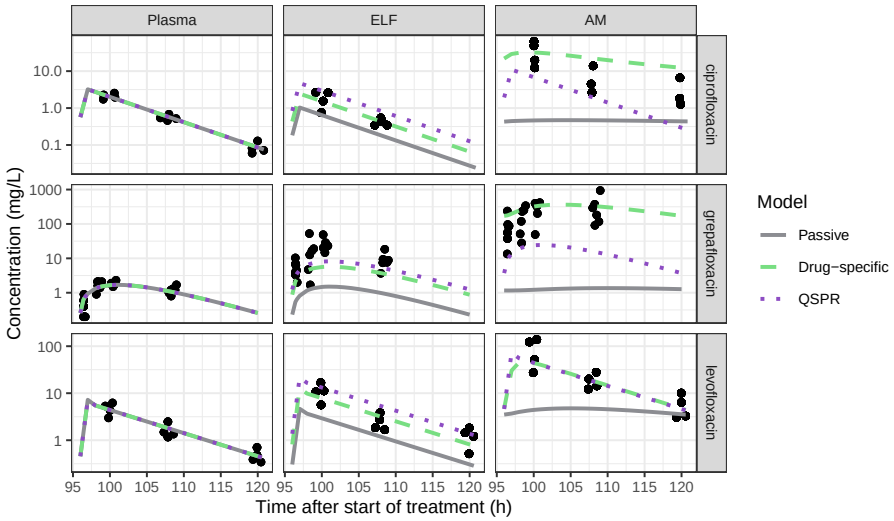

Fig. 4 | Steady-state PK profiles of ciprofloxacin, grepafloxacin, and levofoloxacin. Steady-state ELF and AM PK profiles were evaluated. Observations are shown as dots and model predictions as lines, where the predicted concentration in the pulmonary compartments are the mean of the six lung zones. Three different models were used to predict pulmonary PK; a general passive permeability-limited model (grey solid lines), a drug-specific permeability-limited model (green dashed lines), and a QSPR-informed perfusion-limited model (purple dotted lines).

on AUC, while the C_{max} increased or decreased as a function of Kp_{tissue} for all drugs and compartments except at the AM compartment for the acidic and basic compounds, which remained unaffected. This could be related to the very slow equilibration between the ELF and the AMs for the non-neutral compounds, which leaves changes in the ELF concentration to have less effect on the AM concentration (Fig. S3). In turn, the slow equilibration rate for the basic and acidic compounds could be related to their small neutral fractions (basic: 0.40%, acidic: 0.25%), which is the drug fraction available for transport over the AM membrane. A large impact of decreasing logP values on C_{max} and AUC in AM and ELF compartments was seen. The MW had no impact on the L2R for any of the drug types (data not shown). MW below 85 g/mol was required to pass through the population of small pores (*i.e.*, $r < 0.32$ nm) while the lowest MW simulated was 200 g/mol (equivalent to $r = 0.47$ nm). Similarly, all simulated molecules had free passage through the population of large pores ($r_L = 11.56$ nm). However, the total available surface area was considerable smaller for the large pores compared to the small (0.00079% and 0.303% of the total alveolar surface area, respectively).

We characterized the impact of molecule type (acid, base, or neutral) and logP on predicted time-concentration profiles in plasma, ELF, and AM compartments (**Fig. 5**). Generally, the acidic and neutral compounds showed high agreement between the total AM drug concentration and that the AM cytosol concentration. In these cases, lysosomal trapping has minimal impact on the drug availability at the site of infection (**Fig. 6**). However, for basic compounds, large differences could be seen between the total AM and the cytosolic concentration. Therefore, lysosomal trapping can play a major role for the intercellular PK and if not considered, may lead to the overestimation of antimicrobial

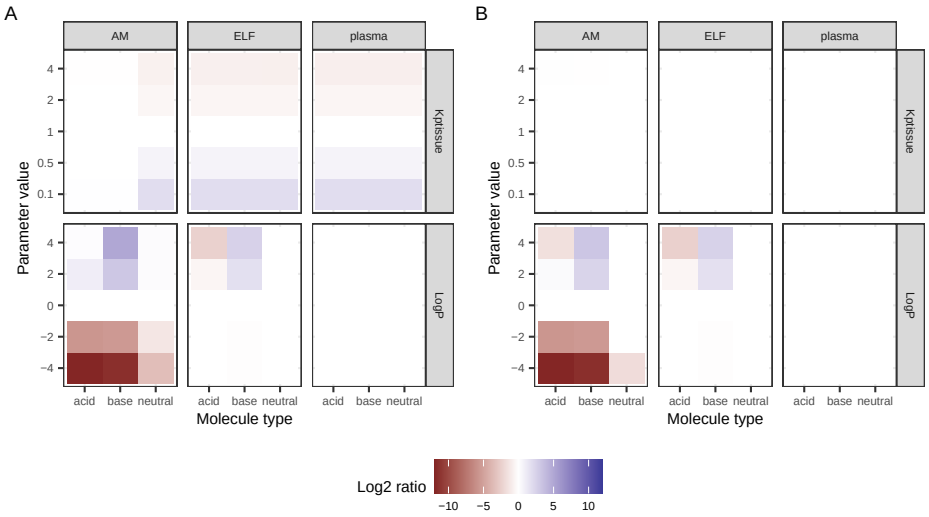

Fig. 5 | Impact of drug-specific parameters on drug exposure. Drug exposure on ELF and AM was evaluated based on **A.** steady state maximum concentration and **B.** 24-hour area under the curve for plasma, ELF, and ELF. The drug-specific parameter altered included tissue partitioning coefficient (Kp_{tissue}), logP, CL and MW (data not shown). The drugs with median parameter values were used as comparator drugs

concentration at the site of action (cytosol).

Pathophysiological effects

Following the sensitivity analysis for drug-specific parameters, we selected acidic, basic, and neutral antimicrobials with a range of logP values (-4, 0, and 4) and a relatively low MW (300 g/mol, $r = 0.57$ nm). Plasma concentrations remained unaffected by the pathophysiological changes simulated (Fig. S4), while the pH of the ELF and interstitium, as well as the size of the pores in the alveolar epithelium, had an effect on the ELF and AM AUC (**Fig. 7**), and a corresponding effect on C_{max} (Fig. S4). The neutral molecules were unaffected by the changes in the system-specific parameters, while the acidic and the basic compound were affected in opposite ways. Drugs of different lipophilicity were affected differently by the pathophysiological changes. Most changes only affect lipophilic drugs (logP = 4). Interestingly, acidification of the ELF affected the more hydrophilic non-neutral compounds (logP 0 or -4). This could be explained by the shift in NF available to pass over the macrophage membrane. The increase of the size of the small pores starts when the radius of the pores exceeds the radius for the molecule. When this occurs, a larger surface area is available for paracellular diffusion. This influences lipophilic molecules, as they diffuse largely *via* transcellular diffusion compared to hydrophilic drugs. Important here is that only the neutral fraction can diffuse over the membrane, while the paracellular route is available without any charge restrictions. When increasing the radius of the small pores, and subsequently the area available for paracellular transport, the ratio between the transcellular and paracellular transport will shift (Fig. S5). Due to the absence of charge restrictions related to the paracellular route, the pH differences between the compartments have less impact. This

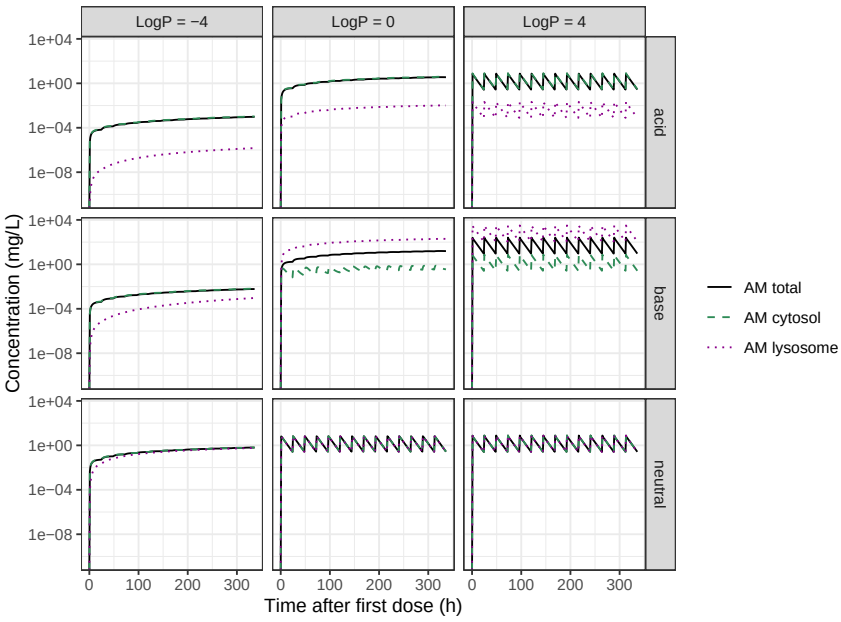

Fig. 6 | Impact of acidity and lipophilicity on drug distribution to the lung compartments. PK of the AM, and their intercellular compartments for nine hypothetical drugs with different acidity and lipophilicity (logP) characteristics were evaluated.

results in a decreased concentration difference between the compartments.

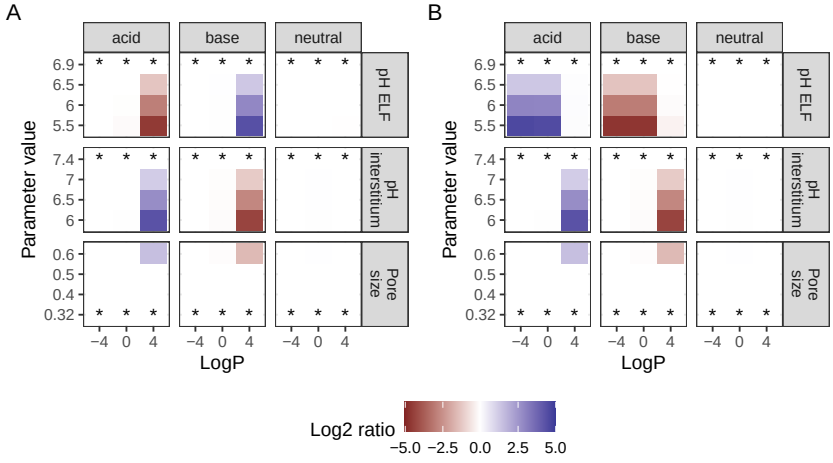

Fig. 7 | Impact of pathophysiological related changes to system-specific parameters. Evaluation was based on the model-predicted steady-state 24-hour area under the concentration-time curve (AUC_{24}) in **A)** ELF and **B)** AM, comparing the effect of pathophysiological changes in system-specific parameters across different drugs. Parameter values of the base scenario are indicated with asterisks (*****).

Discussion

We developed a novel lung PBPK modelling and simulation framework and applied this to study fluoroquinolone PK and investigate the impact of drug specific properties and disease related changes. By comparing the different model-based predictions of pulmonary PK we could identify the importance of considering drug-specific transport, including active processes. Thus, informing the model with permeability data derived from cell-based *in vitro* assays showed to be the best performing approach.

We informed the transport over the alveolar epithelium with permeability data obtained from Calu-3 cell assays. However, such assays are not commonly performed and therefore relevant data are often lacking. In contrast, assays quantifying intestinal permeability are routinely performed for orally administrated drug, primarily using Caco-2 cells. Models predicting Calu-3 permeability based on Caco-2 permeability have been developed[14]. Such models could be incorporated into our framework to allow for simulation of pulmonary PK considering drug-specific transport in the absence of Calu-3 data. However, there are no equivalent translational models for macrophage permeability and currently such data are not commonly available.

The QSPR-based approach, which accounts for active transport processes, was clearly outperforming the approach where only passive diffusion was included (**Fig. 3**). The QSPR-based approach could therefore constitute a relevant alternative to the *in vitro* informed active transport in situations where such data are not available. Due to the flexibility of the developed model, the QSPR-based and *in vitro*-informed approaches could easily be combined. The QSPR approach could be implemented to compensate for missing permeability data for either the alveolar epithelium or the macrophage membrane, depending on data availability.

The modelling framework was used to understand the impact of drug-specific parameters on pulmonary PK. To this end, we used the passive PBPK model. Although this model performed the worst in the model application example, it serves as a useful foundation to pull apart the impact of specific factors on pulmonary PK. We found that lipophilicity was a highly influential drug property in combination with molecular type (*i.e.*, acidic, neutral, basic). Only pathophysiological changes that altered the proportion between transcellular and paracellular transport had an effect on ELF drug exposure, which subsequently altered the AM exposure. The AM exposure was further affected by shifts in the ELF neutral fraction. For acidic compounds, this fraction was increased with increased acidity, and subsequently more drug was available to pass over the AM membrane. As the pH remained the same within the AMs, the fraction available to diffuse back to the ELF was unchanged, resulting in an increase of AM drug concentration. The reverse occurred for the basic compounds. Although we show that lipophilic drugs tend exhibit high grade of lung penetration, there is a high likelihood that such compounds will have poor systemic PK properties and may not reach the lung before they are cleared. This hint towards that targeting lung exposure alone may not be a fruitful approach for systemically administered compounds. To overcome this issue, we see the value of a multifactorial QSPR-PBPK approach in which multiple drug-properties are optimized simultaneously in respect to both systemic and pulmonary PK.

We demonstrate that lysosomal trapping can have a large impact on pulmonary PK. To highlight the relevance of this finding, we can offer a recent example. At the start of the COVID-19 pandemic in 2020, hydroxychloroquine (HCQ) was hypothesized as a potential treatment for COVID-19[32]. HCQ showed *in vitro* efficacy and promising lung tissue distribution, suggesting that HCQ should inhibit coronavirus at clinically feasible

doses[32]. However, HCQ was found ineffective as a COVID treatment[33,34]. The lung-plasma partitioning ratio of HCQ is very high, but this high partitioning was a result of lysosomal trapping[35–37]. Moreover, *in vitro* efficacy had been related to cell culture media concentrations[32], which corresponds to extracellular fluid. The extracellular fluid concentrations in lung tissue were much lower than overall lung tissue, and thus no effective and safe HCQ dosing regimens could be identified. As such, we contend that lysosomal trapping should be explicitly included in lung PK predictions, while at the same time keeping in mind the site of action of the drug.

The developed lung PBPK model constitutes a highly customizable modelling framework. One practical advantage of the framework is that it was developed in the open-source software R[38]. This makes it accessible and flexible, allowing for adjustments of the current model but also the incorporation of model extensions. Therefore, we see this framework as a relevant complementary addition to currently available lung PBPK models implemented in other software packages.

In conclusion, the developed PBPK model framework can support improved characterization of pulmonary exposure of systemically administrated antimicrobials to guide treatment optimization for RTIs.

References

1. Rybak, M. J. (2006). Pharmacodynamics: Relation to antimicrobial resistance. *American Journal of Infection Control*, *34*(5 SUPPL.), 38–45. https://doi.org/10.1016/j.ajic.2006.05.227
2. Rodvold, K. A., Hope, W. W., & Boyd, S. E. (2017). Considerations for effect site pharmacokinetics to estimate drug exposure: Concentrations of antibiotics in the lung. *Current Opinion in Pharmacology*, *36*, 114–123. https://doi.org/10.1016/j.coph.2017.09.019
3. Rodvold, K. A., Yoo, L., & George, J. M. (2011). Penetration of Anti-Infective Agents into PulmonaryEpithelial Lining Fluid. *Clinical Pharmacokinetics*, *50*(11), 689–704. https://doi.org/10.2165/11592900-000000000-00000
4. Huang, Y. C. T., & Piantadosi, C. A. (2002). Alveolar barrier function assessed by hydrophobic and hydrophilic fluorescent solutes in rabbit lung. *Respiratory Physiology and Neurobiology*, *133*(1-2), 153–166. https://doi.org/10.1016/S1569-9048(02)00150-7
5. Brillault, J., De Castro, W. V., & Couet, W. (2010). Relative contributions of active mediated transport and passive diffusion of fluoroquinolones with various lipophilicities in a Calu-3 lung epithelial cell model. *Antimicrobial Agents and Chemotherapy*, *54*(1), 543–545. https://doi.org/10.1128/AAC.00733-09
6. Assmus, F., Houston, J. B., & Galetin, A. (2017). Incorporation of lysosomal sequestration in the mechanistic model for prediction of tissue distribution of basic drugs. *European Journal of Pharmaceutical Sciences*, *109*, 419–430. https://doi.org/10.1016/j.ejps.2017.08.014
7. Bhattacharya, J., & Matthay, M. A. (2013). Regulation and repair of the alveolar-capillary barrier in acute lung injury. *Annual Review of Physiology*, *75*, 593–615. https://doi.org/10.1146/annurev-physiol-030212-183756
8. Peteranderl, C., Sznajder, J. I., Herold, S., & Lecuona, E. (2017). Inflammatory responses regulating alveolar ion transport during pulmonary infections. *Frontiers in Immunology*, *8*, 1–8. https://doi.org/10.3389/fimmu.2017.00446
9. Quinton, L. J., Walkey, A. J., & Mizgerd, J. P. (2018). Integrative physiology of pneumonia. *Physiological Reviews*, *98*(3), 1417–1464. https://doi.org/10.1152/PHYSREV.00032.2017
10. Fischer, H., & Widdicombe, J. H. (2006). Mechanisms of acid and base secretion by the airway epithelium. *Journal of Membrane Biology*, *211*(3), 139–150. https://doi.org/10.1007/s00232-006-0861-0
11. Kiem, S., & Schentag, J. J. (2008). Interpretation of antibiotic concentration ratios measured in epithelial lining fluid. *Antimicrobial Agents and Chemotherapy*, *52*(1), 24–36. https://doi.org/10.1128/AAC.00133-06
12. Välitalo, P. A. J., Griffioen, K., Rizk, M. L., Visser, S. A. G., Danhof, M., Rao, G., van der Graaf, P. H., & van Hasselt, J. G. C. (2016). Structure-Based Prediction of Anti-infective Drug Concentrations in the Human Lung Epithelial Lining Fluid. *Pharmaceutical Research*, *33*(4), 856–867. https://doi.org/10.1007/s11095-015-1832-x

13. Aulin, L. B. S., Valitalo, P. A., Rizk, M. L., Visser, S. A. G., Rao, G., van der Graaf, P. H., & van Hasselt, J. G. C. (2018). Validation of a Model Predicting Anti-infective Lung Penetration in the Epithelial Lining Fluid of Humans. *Pharmaceutical Research*, *35*(2), 26. https://doi.org/10.1007/s11095-017-2336-7
14. Gaohua, L., Wedagedera, J., Small, B. G., Almond, L., Romero, K., Hermann, D., Hanna, D., Jamei, M., & Gardner, I. (2015). Development of a Multicompartment Permeability-Limited Lung PBPK Model and Its Application in Predicting Pulmonary Pharmacokinetics of Antituberculosis Drugs. *CPT: Pharmacometrics and Systems Pharmacology*, *4*(10), 605–613. https://doi.org/10.1002/psp4.12034
15. Eriksson, J., Thörn, H., Lennernäs, H., & Sjögren, E. (2020). Pulmonary drug absorption and systemic exposure in human: Predictions using physiologically based biopharmaceutics modeling. *European Journal of Pharmaceutics and Biopharmaceutics*, *156*, 191–202. https://doi.org/10.1016/j.ejpb.2020.09.004
16. Hartung, N., & Borghardt, J. M. (2020). A mechanistic framework for a priori pharmacokinetic predictions of orally inhaled drugs. *PLoS Computational Biology*, *16*(12 December), 1–24. https://doi.org/10.1371/journal.pcbi.1008466
17. Tylutki, Z., & Polak, S. (2017). A four-compartment PBPK heart model accounting for cardiac metabolism-model development and application. *Scientific Reports*, *7*(June 2016), 1–11. https://doi.org/10.1038/srep39494
18. Krombach, F., Münzing, S., Allmeling, A. M., Gerlach, J. T., Behr, J., & Dörger, M. (1997). Cell size of alveolar macrophages: An interspecies comparison. *Environmental health perspectives*, *105 Suppl*, 1261–1263. https://doi.org/10.1289/ehp.97105s51261
19. Caputo, G. R., Kondo, C., Masui, T., Geraci, S. J., Sullivan, M. M. O., & Higgins, C. B. (1991). Rigth and Left Lung Perfusion : In Vitro and in Vivo Validation with Obliqe-Angle, Velocity-encoded Cine MR Imaging. *Radiology*, *180*, 693–698.
20. BRYAN, A. C., BENTIVOGLIO, L. G., BEEREL, F., MACLEISH, H., ZIDULKA, A., & BATES, D. (1964). Factors Affecting Regional Distribution of Ventilation and Perfusion in the Lung. *Journal of applied physiology*, *19*, 395–402. https://doi.org/10.1152/jappl.1964.19.3.395
21. Grumetto, L., Russo, G., & Barbato, F. (2016). Immobilized Artificial Membrane HPLC Derived Parameters vs PAMPA-BBB Data in Estimating in Situ Measured Blood-Brain Barrier Permeation of Drugs. *Molecular Pharmaceutics*, *13*(8), 2808–2816. https://doi.org/10.1021/acs.molpharmaceut.6b00397
22. Yamamoto, Y., Välitalo, P. A., Huntjens, D. R., Proost, J. H., Vermeulen, A., Krauwinkel, W., Beukers, M. W., Van Den Berg, D. J., Hartman, R., Wong, Y. C., Danhof, M., Van Hasselt, J. G., & De Lange, E. C. (2017). Predicting drug concentration-time profiles in multiple CNS compartments using a comprehensive physiologically-based pharmacokinetic model. *CPT: Pharmacometrics and Systems Pharmacology*, *6*(11), 765–777. https://doi.org/10.1002/psp4.12250
23. Heiskanen, T., Heiskanen, T., & Kairemo, K. (2009). Development of a PBPK Model for Monoclonal Antibodies and Simulation of Human and Mice PBPK of a Radiolabelled Monoclonal Antibody. *Current Pharmaceutical Design*, *15*(9), 988–1007. https://doi.org/10.2174/138161209787581968
24. Van Dyke, R. W. (1993). Acidification of rat liver lysosomes: Quantitation and comparison with endosomes. *American Journal of Physiology - Cell Physiology*, *265*(4 34-4). https://doi.org/10.1152/ajpcell.1993.265.4.c901
25. Johansen, B., Bjortuft, O., & Boe, J. (1993). Static lung volumes in healthy subjects assessed by helium dilution during occlusion of one mainstem bronchus. *Thorax*, *48*(4), 381–384. https://doi.org/10.1136/thx.48.4.381
26. Weibel, E. R. (2017). Lung morphometry: The link between structure and function. *Cell and Tissue Research*, *367*(3), 413–426. https://doi.org/10.1007/s00441-016-2541-4
27. Wiśniewski, J. R., Hein, M. Y., Cox, J., & Mann, M. (2014). A "proteomic ruler" for protein copy number and concentration estimation without spike-in standards. *Molecular and Cellular Proteomics*, *13*(12), 3497–3506. https://doi.org/10.1074/mcp.M113.037309
28. Kim, Y. H., Kim, K. J., D'Argenio, D. Z., & Crandall, E. D. (2021). Characteristics of passive solute transport across primary rat alveolar epithelial cell monolayers. *Membranes*, *11*(5), 1–26. https://doi.org/10.3390/membranes11050331
29. Avdeef, A., Nielsen, P. E., & Tsinman, O. (2004). Pampa - A drug absorption in vitro model: 11. Matching the in vivo unstirred water layer thickness by individual-well stirring in microtitre plates. *European Journal of Pharmaceutical Sciences*, *22*(5), 365–374. https://doi.org/10.1016/j.ejps.2004.04.009
30. Saleh, M. A., Loo, C. F., Elassaiss-Schaap, J., & De Lange, E. C. (2021). Lumbar cerebrospinal fluid-to-brain extracellular fluid surrogacy is context-specific: Insights from LeiCNS-PK3.0 simu-

lations. *Journal of Pharmacokinetics and Pharmacodynamics*, *48*(5), 725–741. https://doi.org/10.1007/s10928-021-09768-7
31. Rodvold, K. A., Danziger, L. H., & Gotfried, M. H. (2003). Steady-state plasma and bronchopulmonary concentrations of intravenous levofloxacin and azithromycin in healthy adults. *Antimicrobial Agents and Chemotherapy*, *47*(8), 2450–2457. https://doi.org/10.1128/AAC.47.8.2450-2457.2003
32. Yao, X., Ye, F., Zhang, M., Cui, C., Huang, B., Niu, P., Liu, X., Zhao, L., Dong, E., Song, C., Zhan, S., Lu, R., Li, H., Tan, W., & Liu, D. (2020). In vitro antiviral activity and projection of optimized dosing design of hydroxychloroquine for the treatment of severe acute respiratory syndrome coronavirus 2 (SARS-CoV-2). *Clinical Infectious Diseases*, *71*(15), 732–739. https://doi.org/10.1093/cid/ciaa237
33. RENKIN, E. M. (1954). Filtration, diffusion, and molecular sieving through porous cellulose membranes. *The Journal of general physiology*, *38*(2), 225–243. https://doi.org/10.1085/jgp.38.2.225
34. Gotfried, M. H., Danziger, L. H., & Rodvold, K. A. (2001). Steady-state plasma and intrapulmonary concentrations of levofloxacin and ciprofloxacin in healthy adult subjects. *Chest*, *119*(4), 1114–1122. https://doi.org/10.1378/chest.119.4.1114
35. Kolli, A. R., Calvino-Martin, F., & Hoeng, J. (2022). Translational Modeling of Chloroquine and Hydroxychloroquine Dosimetry in Human Airways for Treating Viral Respiratory Infections. *Pharmaceutical Research*, 57–73. https://doi.org/10.1007/s11095-021-03152-3
36. Derendorf, H. (2020). Excessive lysosomal ion-trapping of hydroxychloroquine and azithromycin. *International Journal of Antimicrobial Agents*, *55*(6), 106007. https://doi.org/10.1016/j.ijantimicag.2020.106007
37. Wolowich, W. R., & Kwon, Y. M. (2021). Simulation of Drug in the Lung Can Be Misleading. *Clinical Infectious Diseases*, *72*(9), 1677–1678. https://doi.org/https://doi.org/10.1093/cid/ciaa907
38. Team, R. C. (2021). R: A Language and Environment for Statistical Computing.

Supplementary Figures

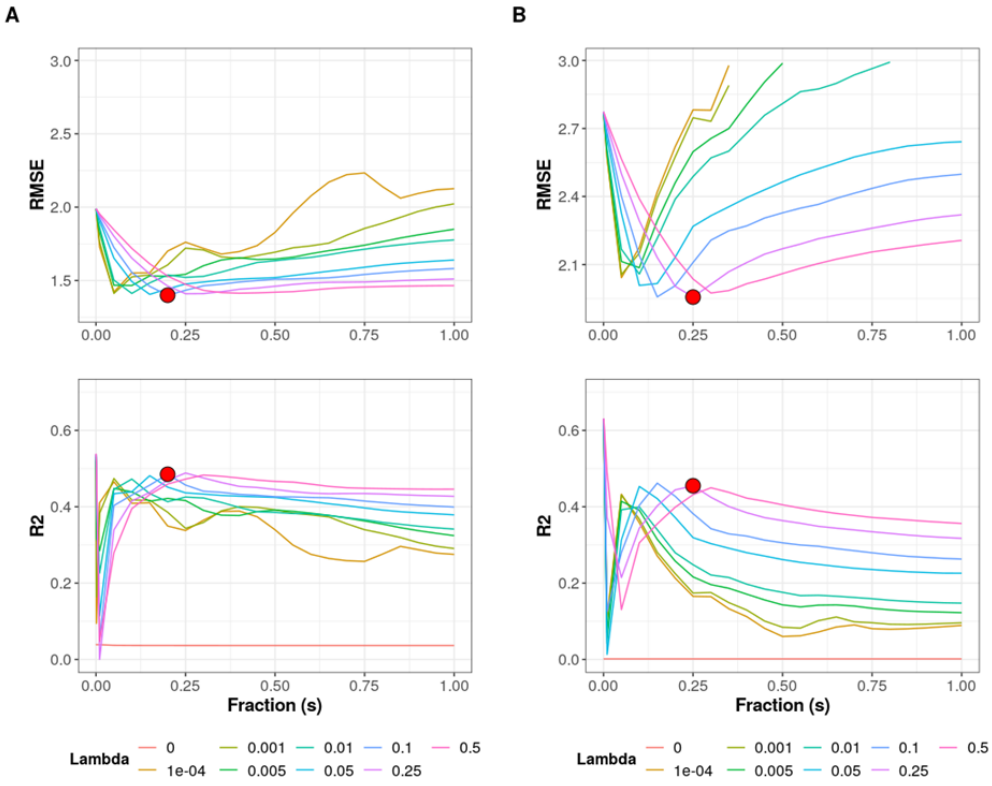

Fig. S1 | Preliminary tuning of elastic net parameters. This preliminary tuning was performed to identify a combination of mixing fraction (s) and shrinkage (λ) values that can minimize RMSE value during elastic net model optimization. Parameter tuning was performed using the leave-one-out cross-validation method and was performed separately for A: EPR and B: MER QSPR models. Parameter values that minimized RMSE in each scenario were indicated by the red dot. This point of RMSE minima corresponded with the r-squared maxima (red dot in the lower panel)

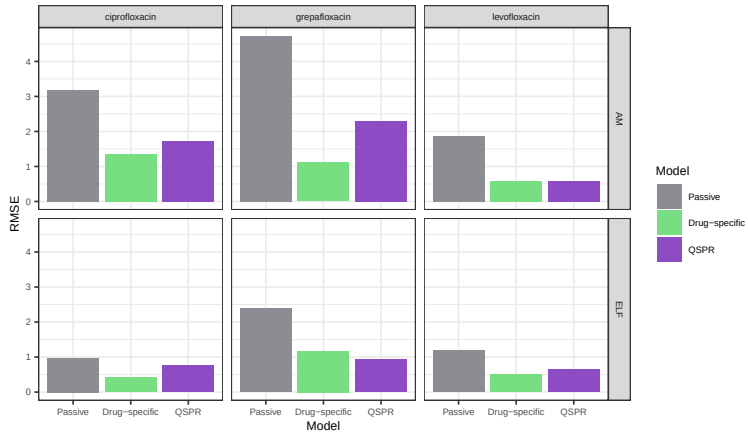

Fig. S2 | Performance comparison of different PBPK models. Comparison of model performance calculated as the root mean squared error (RMSE) for three different variations of the lung sub-model: i) a general passive permeability-limited model, ii) a drug-specific permeability-limited model, iii) a quantitative structure-property relationship (QSPR)-informed perfusion-limited model. The two key pulmonary infection sites were considered, the epithelial lining fluid (ELF) and alveolar macrophages (AM).

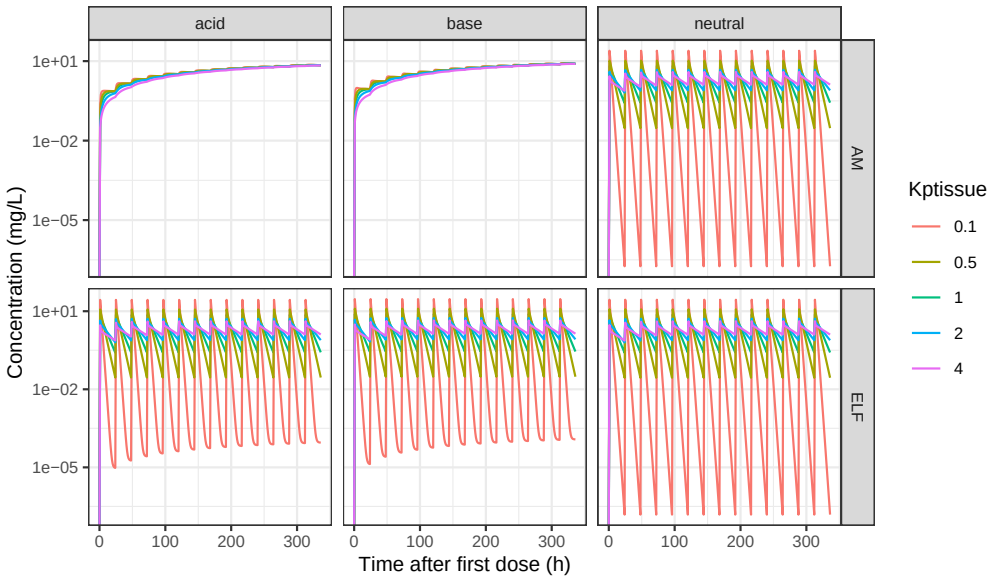

Fig. S3 | Distribution of different hypothetical drugs into the lung compartments. Pharmacokinetics of the epithelial lining fluid (ELF) and alveolar macrophages (AM) of different hypothetical drugs with different partitioning into the peripheral compartment.

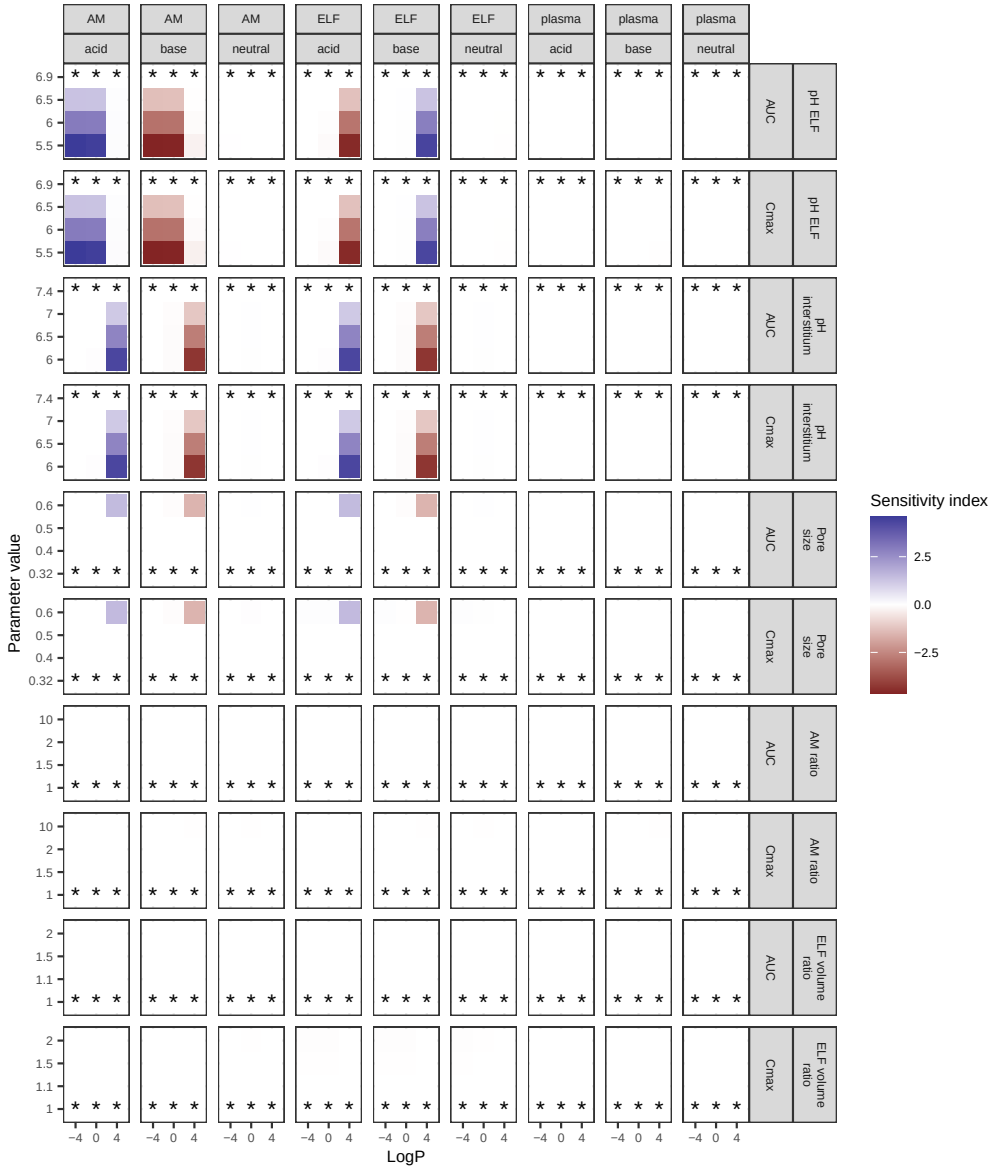

Fig. S4 | Impact of pathophysiological changes on system-specific parameters. The impact of pathophysiological-related changes to system-specific parameters on steady 24-hour area under the curve (AUC) and maximal concentration (C_{max}) for plasma, epithelial lining fluid (ELF) and alveolar macrophages (AM) for different drugs was evaluated. The parameter values of the base scenario are indicated with *.

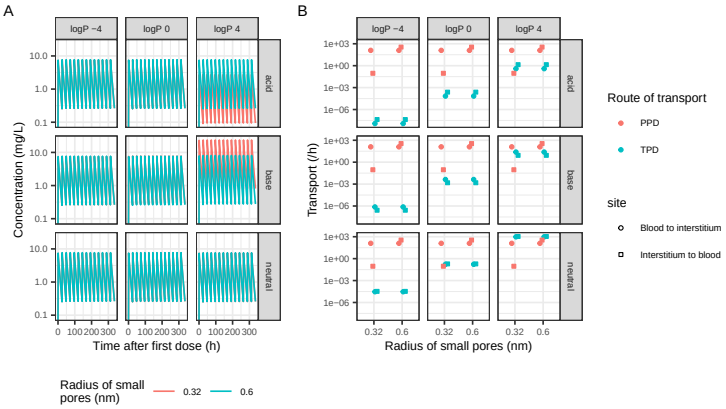

Fig. S5 | Impact of the size of the small pores in the tight junctions in the alveolar epithelium. A. Pharmacokinetics of the epithelial lining fluid (ELF), different hypothetical drugs (facets) with different sizes of the small pores (colour). B. The specific contribution of paracellular (PPD) and transcellular diffusion (TPD) depending on the radius of the small pores and the direction of transport.

Supplementary Table

Table S1. Drug- and study-specific information

	Ciprofloxacin	Grepafloxacin	Levofloxacin
Drug-specific properties			
Parameter			
M_w*	331.34	359.39	361.37
logP*	0.28	0.72	-0.43
pka*	5.76	5.88	5.45
pkb*	8.68	8.77	6.2
Bp	0.7	1.33**[0]	1[0]
$f_{unbound}$[0]	0.65	0.5	0.69
Calu-3 influx ($\times 10^{-6}$ cm/s)	1.03[0]	11.8[0]	6.2[0]
Calu-3 efflux ($\times 10^{-6}$ cm/s)[0]	0.43[0]	3.1[0]	2.4[0]
AM influx ($\times 10^{-6}$ L/min/mg protein)[0]	2.44	28.5	4.11
AM efflux ($\times 10^{-6}$ L/min/mg protein)[0]	0.2	0.67	0.77
Study-specific information			
Study	Gotfried *et al.*[0]	Cook *et al.*[0]	Rodvold *et al.*[0]
Population	Health volunteers	Patients	Health volunteers
Number of subjects	12 (6 M, 6 F)	24 (13 M, 11 F)	12 (5 M, 7 F)
Body weight (kg)	77.3 ± 12.5	71 (45.0–107.5)	78.5 ± 12.0
Mean age (years)	31.2 ± 6.7	57 (27–75)	31.2 ± 10.5
Route of administration	p.o.	p.o.	60 min infusion
Dose (mg)	500	400	500
Dosing regimen	b.i.d.	daily	daily
Last dose given	108 h	96 h	120 h
Subjects per sampling point	4	5–7	4

* Obtained via Drugbank.com
** calculated based on rat data according to Uchimuraa *et al.*[0] using an haematocrit of 45%[0].